A rice tubulin tyrosine ligase-like 12 protein affects the dynamic and orientation of microtubules[∞]

Kunxi Zhang[1]*, Xin Zhu[1], Steffen Durst[1], Petra Hohenberger[1], Min-Jung Han[2], Gynheung An[3], Vaidurya P. Sahi[1], Michael Riemann[1] and Peter Nick[1]

1. Molecular Cell Biology, Botanical Institute, Karlsruhe Institute of Technology, Karlsruhe 76131, Germany
2. Aptamer Initiative, Postech Biotech Center, Pohang University of Science and Technology, Pohang-si, Gyeongsangbuk-do, 37673, South Korea
3. Department of Plant Molecular Systems Biotech, Kyung Hee University, Yongin 446-701, South Korea

*Correspondence: Kunxi Zhang (kunxi.zhang@kit.edu)

Kunxi Zhang

ABSTRACT

The detyrosination/retyrosination cycle is the most common post-translational modification of α-tubulin. Removal of the conserved C-terminal tyrosine of α-tubulin by a still elusive tubulin tyrosine carboxypeptidase, and religation of this tyrosine by a tubulin tyrosine ligase (TTL), are probably common to all eukaryotes. Interestingly, for plants, the only candidates qualifying as potential TTL homologs are the tubulin tyrosine ligase-like 12 proteins. To get insight into the biological functions of these potential TTL homologs, we cloned the rice TTL-like 12 protein (OsTTLL12) and generated overexpression OsTTLL12-RFP lines in both rice and tobacco BY-2 cells. We found, unexpectedly, that overexpression of this OsTTLL12-RFP increased the relative abundance of detyrosinated α-tubulin in both coleoptile and seminal root, correlated with more stable microtubules. This was independent of the respective orientation of cortical microtubule, and followed by correspondingly changing growth of coleoptiles and seminal roots. A perturbed organization of phragmoplast microtubules and disoriented cell walls were further characteristics of this phenotype. Thus, the elevated tubulin detyrosination in consequence of OsTTLL12 overexpression affects structural and dynamic features of microtubules, followed by changes in the axiality of cell plate deposition and, consequently, plant growth.

INTRODUCTION

α- and β- tubulin, the building blocks of microtubules, have been conserved throughout evolution (Little and Seehaus, 1988). They are the target of a number of post-translational modifications (PTMs), including detyrosination, acetylation, or phosphorylation. The modified tubulins are thought to recruit different sets of specific microtubule-associated proteins (MAPs), which have effects on the structural and dynamic properties of microtubules that control specific cellular functions, such as cell division and cell elongation (Nick, 2007; Peris et al., 2009; Cai, 2010).

One of the most common PTMs is the detyrosination/retyrosination cycle. Indeed, in most eukaryotes, almost all α-tubulins harbor a tyrosine as C-terminal amino acid. A tubulin tyrosine carboxypeptidase (TTC, in animal models also abbreviated as TCP) can cleave off this C-terminal tyrosine generating detyrosinated α-tubulin. Subsequently, a tubulin tyrosine ligase

(TTL) can religate a tyrosine to the detyrosinated α-tubulin. The structural analysis of the founder member of TTL from porcine brain (Ersfeld et al., 1993) revealed that TTL preferentially binds to soluble tubulin dimers rather than to polymerized microtubules, and also inhibits the growth rate of microtubules in neurons (Prota et al., 2013). In animal cells, YFP-tagged TTL decorated the mitotic spindle (Barisic et al., 2015). Conversely, suppression of TTL in mice causes perinatal death accompanied by poorly developed neuronal network, which may stem from the mislocalization of the microtubule tip protein CLIP170 (Erck et al., 2005). Recently, the vasohibins (VASHs) and their regulators, the Small Vasohibin Binding Proteins (SVBPs), turned out to be the mammalian TCPs that had remained elusive for 30 years (Aillaud et al., 2017; Nieuwenhuis et al., 2017). However, even in VASH knockout lines, a residual tubulin detyrosination activity persisted, indicating that VASH-independent TCPs must exist as well (Aillaud et al., 2017). Nevertheless, important molecular players of the tubulin detyrosination/retyrosination cycle have been partially identified, which paves way to address the function of this cycle also at the molecular level. However, very little information is available on this cycle in plant cells.

In fixed tobacco cells, both tyrosinated and detyrosinated α-tubulin can be detected in all microtubule arrays through the cell cycle using monoclonal antibodies raised against both tubulin forms. However, detyrosinated α-tubulin was dominant in cortical microtubule-organizing centers (Smertenko et al., 1997). In rapidly cycling cells, where microtubule turnover is high, such as root tip cells of *Pinus radiata* and *Allium cepa*, detyrosinated α-tubulin was not detectable (Gilmer et al., 1999). However, a comprehensive comparison of α-tubulin isoforms in different tissues in *Zea mays* revealed that detyrosinated α-tubulin was found in differentiated tissues of leaves and anthers (Wang et al., 2004), indicating that the abundance of detyrosinated and tyrosinated α-tubulin can be tissue-specific. In addition, signals that change the dynamics of microtubules can shift the ratio between both α-tubulin forms, as shown for gibberellins (Duckett and Lloyd, 1994) or auxin (Wiesler et al., 2002). Taken together, these reports provide the evidence for the presence of detyrosination in plant cells, but also show that this presence depends on cell type, as well as regulating signals.

Unfortunately, the responsible enzymes for the detyrosination/tyrosination cycle have remained cryptic in plants. Especially, VASH or SVBP homologs seem to be lacking, such that our understanding of the plant detyrosination/tyrosination cycle is still in its infancy. Despite the lack of genetic tools for manipulation of these enzymes, pharmacological manipulation has revealed a role of the tubulin detyrosination cycle for plant growth and development. For instance, nitro-tyrosine integrates into detyrosinated α-tubulin by a TTL activity, but resists cleavage by TTC. In fact, by feeding nitro-tyrosine, the ratio of tyrosinated to detyrosinated α-tubulin increased in tobacco BY-2 cells and in rice seedlings, accompanied by decreased mitotic rate, stimulation of cell elongation, and disorientation of cell walls (Jovanovic et al., 2010). This indicates a role of the

detyrosination/tyrosination cycle for cell elongation and cell division. Suppression of detyrosination by parthenolide, a *bona fide* inhibitor of TTC, was shown to stimulate the association of the plant-specific minus-end directed kinesin, KCH, to cortical microtubules. At the same time, phragmoplast microtubules produced a wavy and partially non-contiguous cell plate (Schneider et al., 2015), suggesting that the detyrosination/tyrosination cycle may regulate the recruitment of specific motor proteins to particular arrays of microtubules. A role of this cycle for microtubule organization was also inferred from the observation that reorientation of cortical microtubules in maize coleoptiles induced by auxin depletion involved a transitional step, where transverse microtubules were predominantly tyrosinated, whereas longitudinal microtubules were mainly detyrosinated (Wiesler et al., 2002). These observations link the detyrosination/tyrosination cycle with the spatial organization of specific microtubule arrays, possibly by recruiting specific kinesin motors. Thus, molecular insight into the plant homologs of TTL and TTC is crucial.

Because no homologs of VASHs are present in plants, the plant TTC remains an identified molecular enigma. However, molecular homologs of TTL seem to be present in plant. In animals, TTL protein family contains 1 *bona fide* TTL protein and 13 subgroups referred to TTL-like (TTLL) protein. Among them, the *bona fide* TTL is the only identified enzyme that retyrosinated α-tubulin, while the others are either glutamylases (TTLL1, 2, 4, 5, 6, 7, 9, 11, and 13) or glycylases (TTLL 3, 8, and 10) (Janke and Magiera, 2020). Among those, human TTLL12 represents an atypical TTL family, neither acting as TTL, nor as glutamylase or glycylase, while affecting detyrosination levels. The fact that none of the domains in this protein shows enzymatic activity *in vitro* led to the hypothesis that TTLL12 may be a regulator, rather than an executor of the detyrosination and tyrosination cycle (Wasylyk et al., 2010; Brants et al., 2012). Nevertheless, TTLL12 colocalized with cellular structures containing tubulin, such as midbodies, centrosomes, intercellular bridges, and the mitotic spindle. The TTLL12 family has been reported to be conserved throughout eukaryotes, and seems to be the only clade of the TTL family present in plants (Janke et al., 2005). Because the function of plant TTLL12 proteins is unknown, we wondered whether these proteins may be responsible for detyrosination or tyrosination. Therefore, we cloned TTLL12 from rice, and generated an overexpression line of OsTTLL12-RFP in rice to study its physiological functions in plant growth and development. To address cellular functions during the cell cycle, which is experimentally difficult in rice plants, we also overexpressed OsTTLL12-RFP in tobacco BY-2 cells. We found that OsTTLL12 decorated all microtubule arrays in the tobacco OsTTLL12-RFP overexpressor line, including PPB, spindle microtubules, phragmoplast, and cortical microtubules. Overexpression of OsTTLL12-RFP increased the resistance of roots to oryzalin treatment and caused altered growth patterns of coleoptiles and roots, correlated with changes in the orientation of cortical microtubules. Moreover, overexpression of

OsTTLL12 partitioned α-tubulin to the detyrosinated state, in both rice plants (coleoptile and root) and tobacco BY-2 cells. Overexpression of OsTTLL12-RFP in rice led to disoriented cross walls in the root apex. In the BY-2 overexpressor, we observed a wavy and not contiguous phragmoplast. Thus, perturbed tubulin detyrosination affected the formation of phragmoplast microtubules and cross-wall deposition.

RESULTS

Phylogenetic analysis of plant TTLL12

All α-tubulins from plants harbor the C-terminal tyrosine that can be removed by unidentified TTC, generating detyrosinated α-tubulin and the tyrosine can be religated to detyrosianted α-tubulin by TTL, yielding tyrosinated α-tubulin (Figure 1A). To study the function of this detyrosination/retyrosination cycle, we searched for putative plant homologs of TTL. In fact, we

recovered TTL-like 12 (TTLL12) proteins in plants that aligned with deduced protein sequences of TTLL12 from plants and animals as well as putative TTLs from animal. The three homologs of TTLL12 proteins in rice: a hypothetical protein without annotated function (SwissProt accession no. Q8H022, OSJNBa0050H14.8, rice 1), two proteins annotated as TTL-like 12 proteins (SwissProt accession no. Q10QY4, LOC_Os03g08140.1, rice 2 and SwissProt accession no. Q10QY3, LOC_Os03g08140.2, rice 3) harbored a TTL domain in their C-terminal region between amino-acid residue 534 and 862 (Figure S1), which was conserved among *Arabidopsis thaliana*, *Vitis vinifera*, and *Physcomitrella patens*. Furthermore, all tested plant TTLL12s showed a long N-terminal extension containing a leucin-rich repeat (LRR) domain (Figure S1), which was absent from putative animal TTLs.

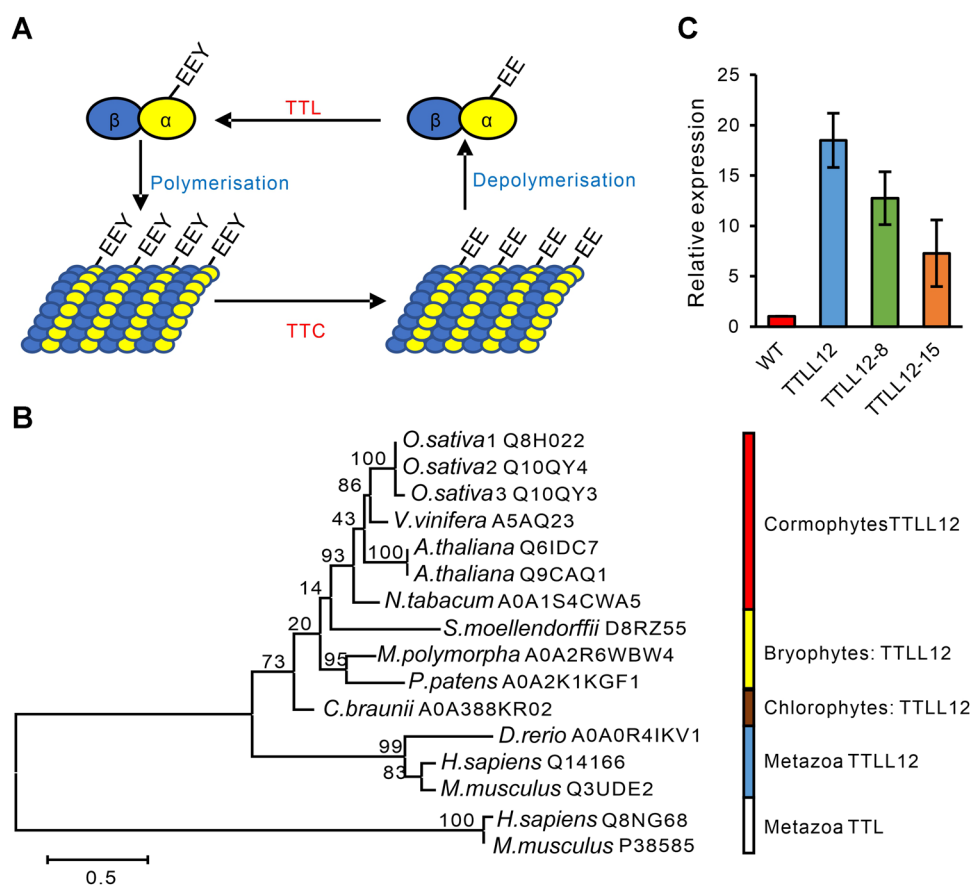To infer the phylogenetic relationship, two sequences of putative TTL from animals and 14 deduced amino acid

Figure 1. Phylogenetic analysis of plant TTLL12 and relative expression levels of OsTTLL12 in overexpression of OsTTLL12 lines
(**A**) Schematic for detyrosination and tyrosination cycle of α-tubulin. Almost all eukaryotic α-tubulins can encode the tyrosine (Y) in their C-terminals, which assemble into microtubules generating tyrosinated microtubules upon polymerization. This C-terminal tyrosine on the surface of microtubules can be enzymatically cleaved off by tubulin tyrosine carboxypeptidase (TTC), yielding detyrosinated microtubules. Later, when α/β-heterodimers detach from microtubules upon depolymerization, the detyrosinated α-tubulin can be religated by tubulin tyrosine ligase (TTL), generating tyrosinated α-tubulin, which is ready for the next round of polymerization. (**B**) Position of rice OsTTLL12s in a phylogeny constructed by neighbor joining based on 16 TTL homologs from plants and animals. Rice has three homologs of TTL family protein – Q8H022, Q10QY4, and Q10QY3 – as TTL-like 12 proteins. (**C**) Steady-state transcript levels of OsTTLL12 in primary roots of different overexpressor rice lines as compared with the non-transformed wild type (WT). Data represent mean values $\pm$ *SE* from three biological replicates.

sequences of TTLL12 from plants and animals were analyzed by the neighbor-joining (NJ) algorithm. As shown in Figure 1B, the phylogenetic tree was found to be divided into two main branches: the two representative sequences of TTL from metazoan animals (*Homo sapiens*, Q8NG68; *Mus musculus*, P38585) clearly clustered into a separate group, while all deduced sequences of TTLL12 from plants and animals clustered into one clade. Within the TTLL12 clade, plant TTLL12s clearly separate from the representatives of metazoan animals (*Danio rerio*, *H. sapiens*, *M. musculus*). Within the plant clade, the Angiosperms were forming a subclade supported by a high bootstrap value (93%), the Lycophyte *Selaginella moellendorfii* stood basal to this clade, while the two tested Bryophytes (*Marchantia polymorpha* and *P. patens*) grouped into a well-supported (bootstrap value of 95%) own subclade. As representative of the Chlorophytes, a sequence from *Chara braunii* could be recovered that located at the base of the plant clade, but remained clearly distinct (with a bootstrap value of 73%) from the metazoan clade.

Generation of rice TTLL12-RFP overexpressor lines

To get insight into the function of rice TTLL12, we generated rice and tobacco BY-2 overexpression lines by cloning OsTTLL12 (Q10QY4, LOC_Os03g08140.1, rice 2) under control of the CaMV-35S promotor as fusion with a monomeric Red Fluorescent Protein N-terminal of the coding sequence. Twenty independent lines confirmed by genotyping and microscopic validation of the RFP marker were raised by self-pollination over so far four subsequent generations to ensure genetic homogeneity. From these, three lines with variable expression levels as probed by quantitative real-time polymerase chain reaction (RT-qPCR) were selected (Figure 1C). Compared with the wild type (WT), steady-state transcript levels in these lines probed in the seminal root were elevated by 17, 12, and 7 times, respectively. All three overexpression lines showed longer coleoptile but shorter primary roots (Figure S2) and disoriented cell walls (Figure 7). Furthermore, the root width was more resistant to oryzalin treatment (Figure S3). Therefore, these phenotypes were comparable over all three overexpression lines and we selected the overexpression rice line with highest expression for further study and referred to this line as OsTTLL12.

OsTTLL12-RFP decorates all microtubule arrays

In order to understand the potential function of OsTTLL12, the cellular localization of its RFP fusion was checked upon overexpression in tobacco BY-2 cells. We found the RFP signals localized in the cytoplasm (Figure S4A). To see whether the excessive protein from the overexpression might mask the true localization, we used an immunofluorescence approach, because the permeabilization of the membrane should wash out unbound protein. Therefore, we followed the RFP signal with respect to microtubules visualized by indirect immunofluorescence (using the mouse monoclonal anti-α-tubulin antibody DM1A conjugated with fluorescein isothiocyanate (FITC) as readout) through the cell cycle. Now, we were able to observe that OsTTLL12 colocalized with all

microtubule arrays, including cortical microtubules in interphase cells, preprophase band and nuclear rim at the G2/M transition, spindle microtubules at anaphase, and the phragmoplast during telophase (Figure 2A), with no obvious preference for specific subsets of microtubules. We found a similar situation also in the homologous system, rice. In living apical meristem zone of the OsTTLL12 root, the RFP signals was also localized in the cytoplasm (Figure S4B). However, association with specific arrays of cortical microtubules became manifest upon immunofluorescence, when cytoplasmic proteins are mostly washed out in consequence of permeabilization and sectioning. When microtubules were visualized by immunofluorescence in root sections from OsTTLL12, we observed a clear asymmetry for the two signals (Figure 2B). While the dense and obliquely oriented cortical microtubules in the rhizodermal layer showed a strong label for DM1A, but seemed not decorated by RFP-OsTTLL12, the pattern was inverse for the cells of the subtending cortex layer, where microtubules were organized in transverse and looser arrays and were not recognized by DM1A, but clearly decorated by RFP-OsTTLL12.

Overexpression of OsTTLL12 modulates orientation of microtubules, cell elongation, and cell division

We found that overexpression of OsTTLL12 stimulated coleoptile growth, but repressed root growth in the seedling stage (Figures 3A, B, S2), which could be observed over 14 d growth, where overexpression of OsTTLL12 promoted plant height but restrained root growth (Figure S5A, B). Even in adult plants, after 60 d of growth, the overexpressor showed a distinct phenotype with a reduced apical dominance (Figure S5C). However, the tiller angle became narrower due to overexpression of OsTTLL12 (Figure S5D).

After germination, rice coleoptiles grow exclusively by cell expansion, while for the rice root, growth starts with cell division in the meristem, followed by cell elongation in the elongation zone and, eventually, cell differentiation in the maturation zone. Importantly, cell division and expansion depend on different arrays of microtubules (Nick, 2007). In addition, detyrosination levels differ depending on the orientation of cortical microtubules (Wiesler et al., 2002). Therefore, we asked the question whether the overexpression of OsTTLL12 would correlate with changes of microtubule orientation and, consequently, changes of organ growth.

After completion of coleoptile expansion, at day 6 after sowing, coleoptiles in OsTTLL12 overexpressor appeared to be longer than in WT (Figure 3A). In fact, average length of coleoptiles was significantly increased by 28% (Figure 3D, left). To find out whether the longer coleoptile in OsTTLL12 overexpressor was due to enhanced cell expansion or increased cell number, mean cell length and cell number were determined from epidermal cells over the entire length of the coleoptile. As shown in Figure 3E, the mean cell length in OsTTLL12 overexpressor clearly exceeded that of the WT, while the mean cell number in OsTTLL12 overexpressor was lower compared with the WT. The difference in elongation was
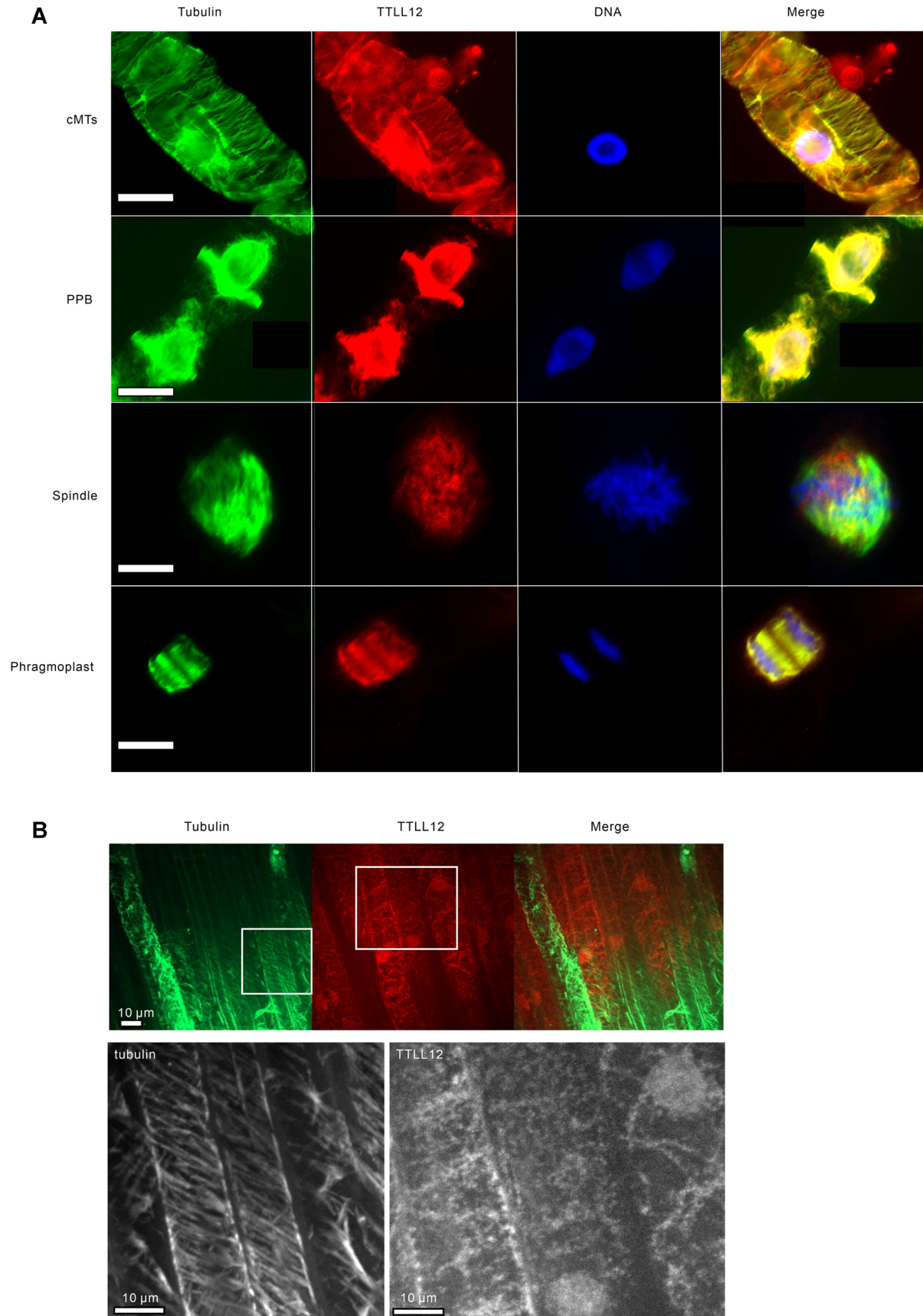
A

	Tubulin	TTLL12	DNA	Merge
cMTs				
PPB				
Spindle				
Phragmoplast				

B

Tubulin   TTLL12   Merge

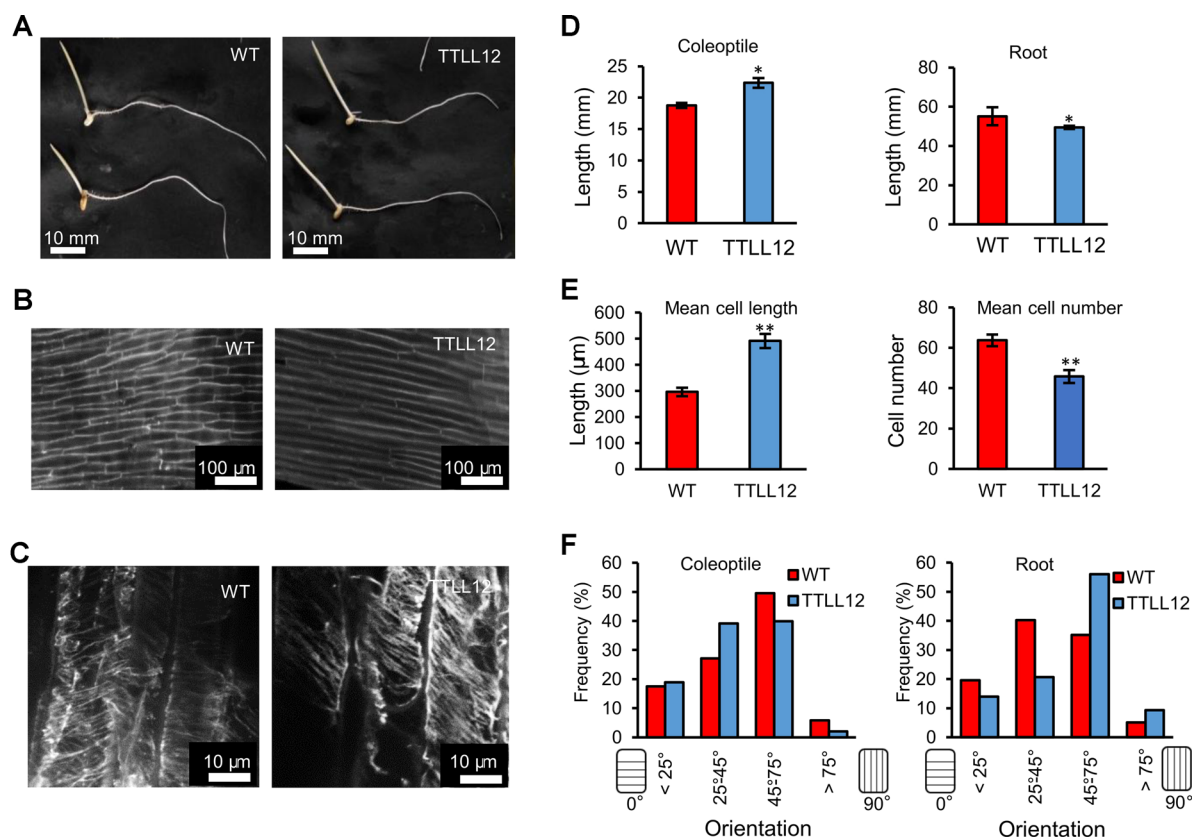tubulin   TTLL12

Figure 2. Continued.

Figure 3. Overexpression of OsTTLL12-RFP caused phenotypical alteration and microtubules reorientation

(**A**) Representative images of root and coleoptile of wild type (WT) (left) and OsTTLL12 overexpressor (right) after 6 d of germination. Bar, 10 mm. (**B**) Representative images of epidermis cells visualized by the autofluorescence of their cell walls in the coleoptile base of WT and OsTTLL12 overexpressor. Bar, 100 μm. (**C**) Representative images of microtubules orientation in the root of WT and OsTTLL12 overexpressor. Microtubules were visualized by immunofluorescence using a fluorescein isothiocyanate (FITC)-conjugated secondary antibody. Bar, 10 μm. (**D**) Coleoptile and root length of WT and OsTTLL12 overexpressor. (**E**) Mean cell length and mean cell number of coleoptiles in WT and OsTTLL12 overexpressor. Data represent mean values ± *SE* of three replicates and each replicate contains a total of at least 350 analyzed cell files collected from 15 individual coleoptiles and root. Asterisks (**) indicate significant differences ($P < 0.01$) between WT and OsTTLL12 overexpressor as assessed by a *t*-test for unpaired data. (**F**) Frequency distributions over microtubule orientation in epidermis of coleoptile and seminal root elongation zone. The angle of microtubule is defined as 0° when microtubule perpendicular to the side wall, whereas 90° represented microtubule parallel to the side wall. The frequency of microtubule orientation was quantified in total of 435 cells of WT and 450 cells of OsTTLL12 overexpressor in four biological replicates.

most pronounced in the basal part of the coleoptile (Figure 3B), where the cells of OsTTLL12 overexpressor appeared extremely long and rectangular, while WT cells of the same region were much shorter and still more rhomboid in shape. Thus, the observed increment in coleoptile length results from a strong stimulation of cell elongation in the OsTTLL12 overexpressor. A concomitant strong decrease in cell number compensates the resulting increase, but only partially. To find out whether the stimulated cell elongation by overexpression of OsTTLL12 correlates with a changed orientation of cortical microtubules, we visualized the cortical microtubules of epidermal cells at day 6 by immunofluorescence and constructed frequency distributions over orientation (Figure 3F). Here, for coleoptiles from the OsTTLL12 overexpressor, the distribution was shifted towards the left as compared with the WT, which means that microtubules assumed more shallow angles with the short cell axis, while in the WT microtubules were mostly oriented in steeply oblique arrays.

In contrast to the coleoptile, the seminal root was shorter in OsTTLL12 overexpressor as compared with the WT

Figure 2. Subcellular localization of OsTTLL12 in cycling and non-cycling cells

(**A**) Localization of OsTTLL12-RFP in tobacco BY-2 cells overexpressing OsTTLL12-RFP in relation to the different microtubule arrays seen during the cell cycle (cortical microtubules, PPB, spindle, and phragmoplast). Microtubules are visualized by immunofluorescence using antibody DM1A, fluorescein isothiocyanate (FITC) as a marker; OsTTLL12 is visualized by the signal from RFP; DNA visualized by Höchst 33258. Bar, 20 μm. (**B**) Double staining of OsTTLL12-RFP in the outermost cell layers (rhizodermis and root cortex) of seminal roots in relation to cortical microtubules. The insets show high magnification of rhizodermis and root cortex. Bar, 10 μm.

(Figure 3A, D). In order to test whether the difference of root growth between WT and OsTTLL12 overexpressor was related to potential differences of microtubule orientation in the cortex of the root elongation zone, we visualized microtubules in longitudinal sections by immunofluorescence at the same time point, at day 6 after sowing and constructed again frequency distributions over microtubule orientation. In the WT, cortical microtubules were mostly transverse or slightly oblique, while in OsTTLL12 overexpressor, their orientation appeared shifted to steeper angles (Figure 3C). The frequency distributions supported this impression (Figure 3F). Here, for roots of OsTTLL12 overexpressor, the distribution was shifted towards the right as compared with the WT, which means that microtubules assumed steeper angles with the short cell axis, while in the WT microtubules were mostly oriented in shallower arrays.

Thus, the effect of OsTTLL12 overexpression on organ growth is just opposite for coleoptiles and seminal roots. However, in both cases, the shift in the orientation of cortical microtubules correlated tightly with the shift of growth: for coleoptiles, microtubules became transverse in the overexpressor accompanied by an increase of growth, for the seminal roots, microtubules became more longitudinal in the overexpressor accompanied by a decrease of growth.

Overexpression of OsTTLL12 confers a reduced sensitivity to oryzalin

Because the stability of microtubules correlates (among other factors) with the abundance of detyrosinated α-tubulin, we wondered whether microtubule dynamics would increase upon overexpression of OsTTLL12. This should become physiologically manifest as an increased sensitivity towards oryzalin, a dinitroaniline herbicide that sequesters tubulin dimers and, thus, eliminates microtubules depending on their innate turnover. As shown in Figure S3A, 100 nmol/L oryzalin treatment resulted in swollen root tips in WT and three overexpression of OsTTLL12-RFP rice lines. However, compared with WT, the root tips were less affected upon oryzalin treatment as evident from narrower roots in presence of oryzalin in the three tested overexpression lines (Figure S3B). Moreover, oryzalin arrested root growth. Without oryzalin, primary root length of WT increased from around 5.8 to 6.9 cm, and primary root length of OsTTLL12 increased from around 4.1 to 4.8 cm. However, upon 100 nmol/L oryzalin treatment, primary root length of WT only increased from 5.6 to 5.9 cm whereas OsTTLL12 increased from 3.8 to 4.2 cm (Figure 4A). Furthermore, in the absence of oryzalin, the growth rates were identical (~19% per day; note that overall root length in the overexpressor did not catch up, because the WT had kept this growth rate over a longer time interval). As expected, the
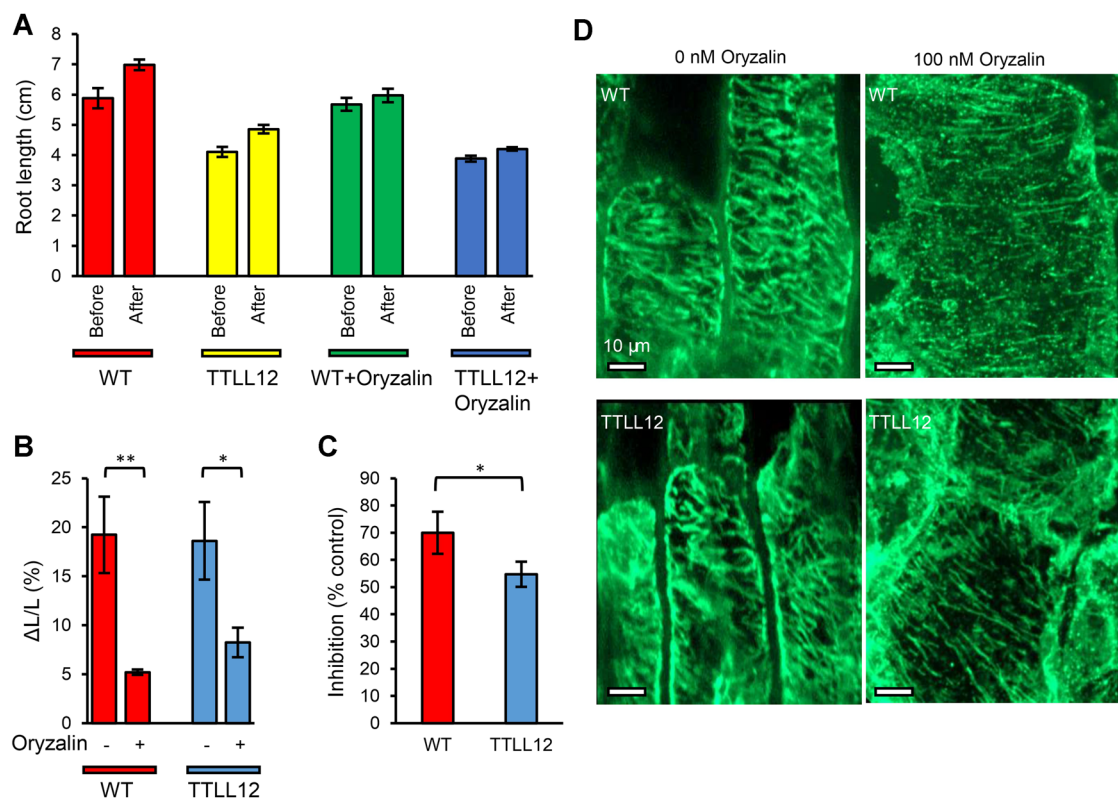

Figure 4. Overexpression of OsTTLL12-RFP conveyed more resistance to oryzalin treatment
(A) Absolute length of primary roots of wild type (WT) and OsTTLL12 seedlings before and after treatment with or without 100 nmol/L oryzalin. (B) Comparison of relative growth rate of seminal roots between WT and OsTTLL12 seedlings after treatment with 100 nmol/L oryzalin. (C) Comparison of relative inhibition of root growth between WT and OsTTLL12 overexpressor seedlings after treatment with 100 nmol/L oryzalin. Asterisks (**) indicate significant differences ($P < 0.01$) from three independent replicates in t-tests for paired data and each replicate represents nine seedlings. (D). Comparison of microtubules in root sections of WT and OsTTLL12 visualized by immunofluorescence staining with and without treatment of 100 nmol/L oryzalin.

growth rates of both roots of WT and OsTTLL12 overexpressor decreased significantly in the presence of 100 nmol/L oryzalin (Figure 4B). However, this reduction was significantly stronger in the WT (from 19.2% to 5.2%, corresponding to 70% inhibition, Figure 4C) when compared with OsTTLL12 overexpressor (from 19.2% to 8.2%, corresponding to only 55% inhibition, Figure 4C). These reductions were accompanied by a more severe disintegration of microtubules (Figure 4D). Without oryzalin treatment, the integrity of microtubules was almost the same in root of WT and OsTTLL12. However, after 100 nmol/L oryzalin treatment, most of the microtubules in the WT vanished down to punctate signals, probably representing microtubule-organizing centers; only some rod-like fragments remained, whereas in OsTTLL12 most of the microtubules still presented longer fragments.

Thus, the roots of the OsTTLL12 overexpressor did not show the expected increase in oryzalin sensitivity, but a significant decrease.

Overexpression of OsTTLL12 shifts α-tubulin into the detyrosinated form

The overexpression of OsTTLL12-RFP should modulate the partitioning between tyrosinated and detyrosinated α-tubulin. To test this implication from a potential function in the tubulin/tyrosine cycle, we extracted total proteins from coleoptiles and

roots of WT and OsTTLL12 overexpressor at day 6 after sowing. Upon separation by sodium dodecyl sulfate polyacrylamide gel electrophoresis (SDS-PAGE; Figure 5A, C, CBB) and probing by western blotting using two monoclonal antibodies – ATT, detecting tyrosinated α-tubulin (Figure 5A, C, tyr-tubulin), and DM1A, detecting detyrosinated α-tubulin (Figure 5A, C, detyr-tubulin) – we quantified the resulting signals and compared them on a relative scale (Figure 5B, D). In coleoptiles, the relative content of tyrosinated α-tubulin did not change upon overexpression of OsTTLL12, while the relative content of detyrosinated α-tubulin increased by 70% in OsTTLL12 overexpressor compared with the WT (Figure 5B). In roots, we found the same phenomenon of an increased detyrosinated α-tubulin content, albeit less pronounced (Figure 5D). Here, the value for OsTTLL12 overexpressor was 30% higher when compared with the WT. Again, there was no difference of tyrosinated α-tubulin between the roots from WT and OsTTLL12 (Figure 5D). In conclusion, overexpression of OsTTLL12 did not lead to higher proportions of tyrosinated α-tubulin, but, opposite to the expectation, increased detyrosinated α-tubulin content in both coleoptile and root. We found the same pattern also in BY-2 cells overexpressing of OsTTLL12 (Figure S6). Here, the upper band detected by ATT representing tyrosinated α-tubulin was stronger in WT BY-2 cells, while the (somewhat smaller) band detected by DM1A
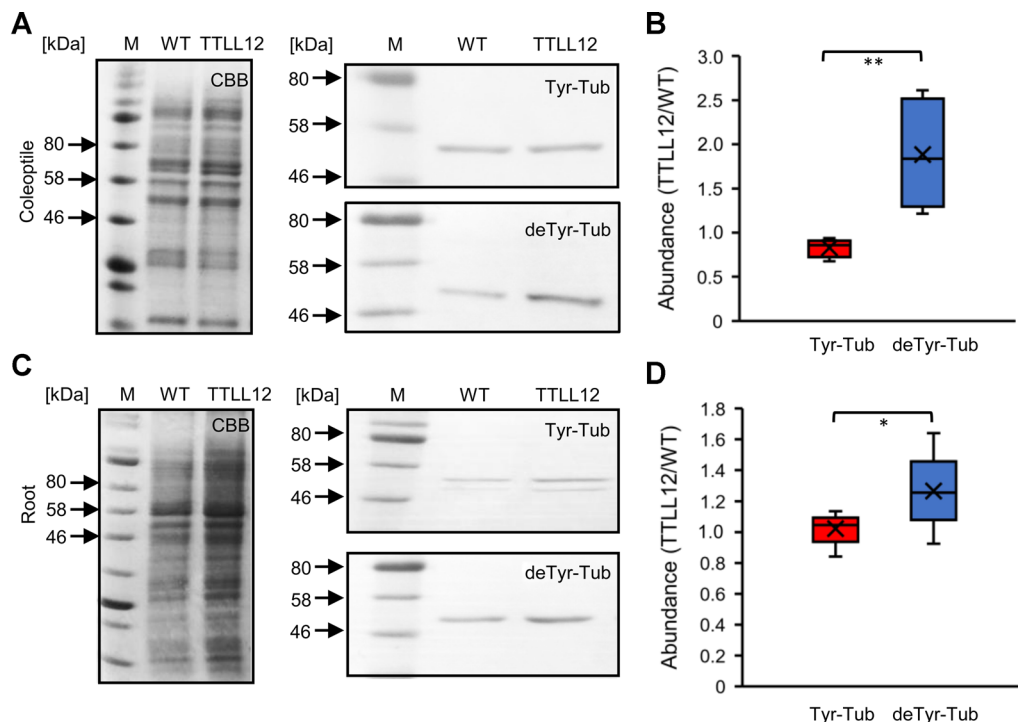

Figure 5. Detection of tyrosinated and detyrosinated α-tubulin by antibodies ATT and DM1A in total extracts from coleoptiles and seminal roots of wild type (WT) and OsTTLL12 overexpressor at day 6 after germination
(A) and (C) Representative images of western blots obtained from coleoptile and root extracts. Left, Coomassie Blue stained gel (CBB); right, tyrosinated α-tubulin detected by ATT (upper part), and detyrosinated α-tubulin detected by DM1A (lower part). Boxplot of relative content of tyrosinated (Tyr-tub) and detyrosinated (deTyr-tub) α-tubulin in (B) coleoptiles or (D) seminal roots of the OsTTLL12 overexpressor in comparison to the WT (defined as 1). The box shows the interquartile range of the coefficient of variability with the inner line in the box indicating the median and × representing mean values. Data are collected from six biological replicates of coleoptile and five replicates of root.
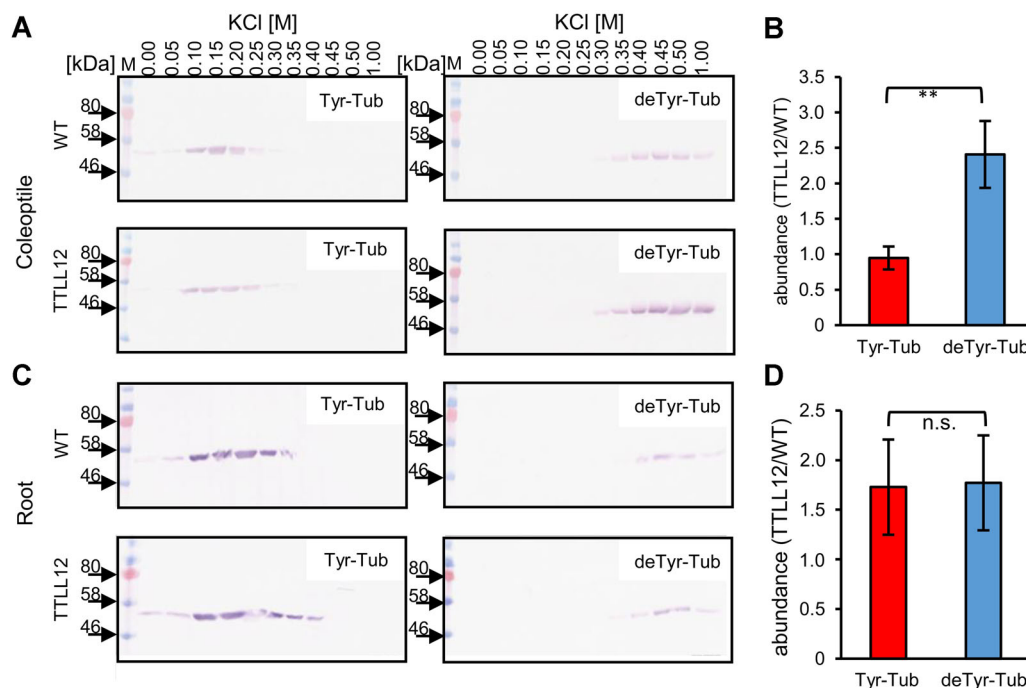
Figure 6. Separation of tyrosinated and detyrosinated α-tubulin in extracts from coleoptile and root of wild type (WT) and OsTTLL12 by ethyl-*N*-phenylcarbamate (EPC) sepharose affinity chromatography
(**A**) and (**C**) Representative images of tyrosinated α-tubulin (detected by ATT) and detyrosinated α-tubulin (detected by DM1A) in the fractions from coleoptile and root extracts eluted by a gradient of concentrations of KCl. (**B**) and (**D**) Quantification of tyrosinated and detyrosinated α-tubulin content from coleoptiles and seminal roots of OsTTLL12 overexpressor relative to WT (defined as 1). Data represent mean values ± *SE* of three replicates from coleoptile and root.

representing detyrosinated α-tubulin was stronger in the line overexpressing of OsTTLL12.

In order to further validate the perturbed ratio of tyrosinated/detyrosinated α-tubulin seen in the OsTTLL12 overexpressor, we employed ethyl-*N*-phenylcarbamate (EPC) affinity chromatography to separate tyrosinated and detyrosinated α-tubulin in a single step, due to a higher affinity of detyrosinated α-tubulin for this antimicrotubular compound (Wiesler et al., 2002). After incubation of coleoptile (Figure 6A, B) and root (Figure 6C, D) extracts with EPC sepharose, the bound proteins were eluted by a gradient of increasing ionic strength, and the fractions were collected, separated by SDS-PAGE, transferred to a membrane, and probed by antibodies ATT (directed to tyrosinated α-tubulin) and DM1A (directed to detyrosinated α-tubulin). Tyrosinated α-tubulin detected by ATT had a lower affinity with EPC sepharose and could be eluted at lower ionic stringency, by lower concentrations of KCl (Figure 6A, C, tyr-Tub), whereas detyrosinated α-tubulin could only be eluted by higher concentration of KCl (Figure 6A, C, detyr-Tub), which was consistent with a previous report (Wiesler et al., 2002). The signals detected by ATT and DM1A were quantified (Figure 6B, D). In coleoptiles of OsTTLL12 overexpressor (Figure 6B), the abundance of tyrosinated α-tubulin was the same as in the WT, while the abundance of detyrosinated α-tubulin was strongly increased (with a surplus of 150% for coleoptiles over the values found in the WT). In the roots (Figure 6D),

both the abundance of tyrosinated α-tubulin as well as of detyrosinated α-tubulin were increased by 70% in OsTTLL12 overexpressor, as compared with the WT. However, the ratio of both tubulin forms was not significantly different. In summary, the more sensitive approach to purify the two tubulin pools by affinity chromatography, confirmed that tubulin in coleoptiles of OsTTLL12 overexpressor was significantly more detyrosinated, while tyrosinated α-tubulin remained at the same level as in the WT (note: it did not decrease to compensate the higher level of detyrosinated tubulin). In the root, the situation differed: here, both pools of tubulin increased to the same degree over the values seen in the WT.

Overexpression of OsTTLL12 leads to disoriented cross walls and affects phragmoplast organization
To get insight into the reduced root growth in OsTTLL12 overexpressor (Figure 3D), the apical region of the seminal root was stained with propidium iodide at day 6 after sowing to visualize the cell walls for confocal microscopy. Here, the transition zone between meristem and distal elongation zone displayed a distinct and specific phenotype (Figure 7A): while in the WT cross walls were strictly perpendicular with the root axis, and evenly spaced, in the overexpressor they were oblique, in some cases even curved, and spaced unevenly. We found this phenotype in all tested lines overexpressing of OsTTLL12 (Figure 7A). A frequency distribution constructed over the incidence of normally and abnormally oriented cell wall (Figure 7B, C) confirmed that
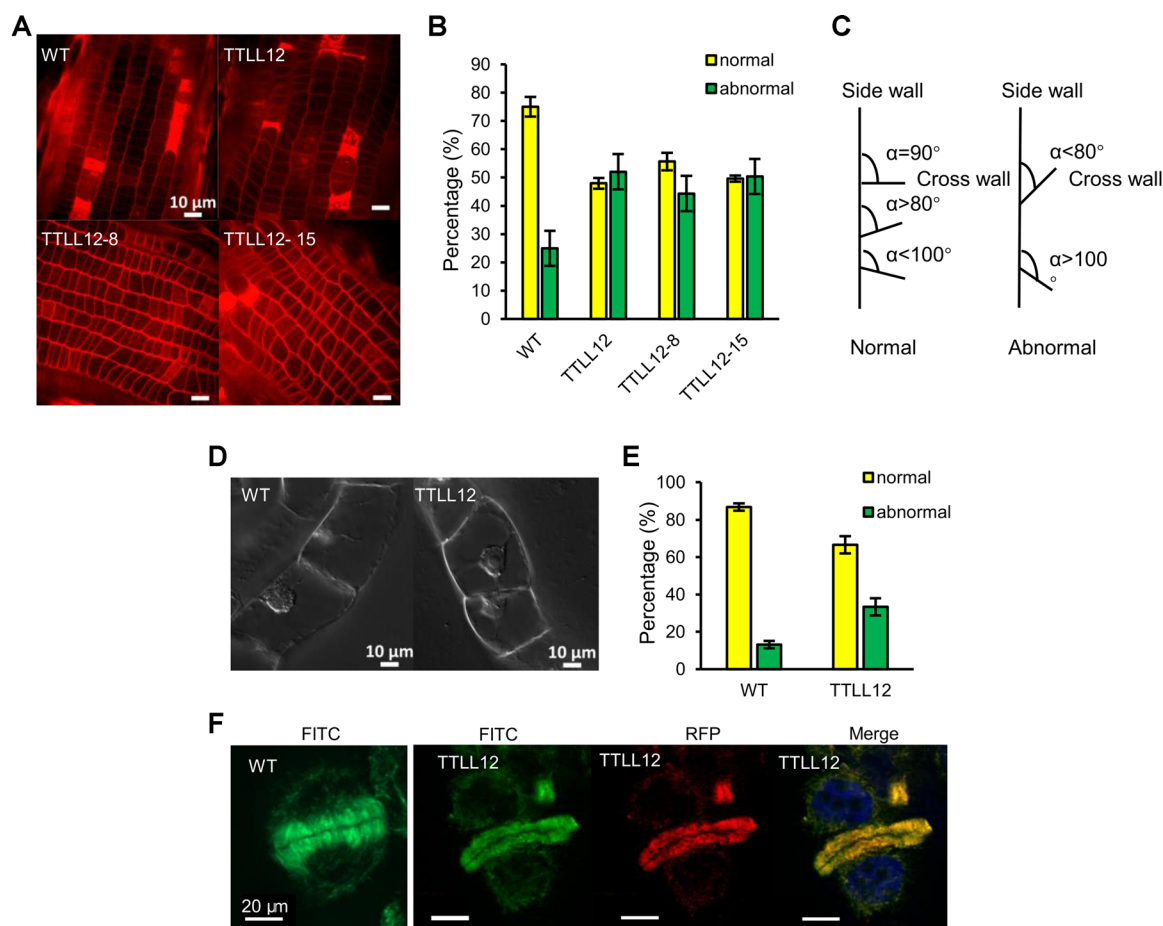
Figure 7. Overexpression of OsTTLL12-RFP disorients cell walls and phragmoplast microtubules organization

(**A**) Representative images of cell walls in the root apex stained by propidium iodide in different overexpression of OsTTLL12 rice lines and wild type (WT). (**B**) Frequency distribution over the orientation of cross walls in the root apex; data represent mean values $\pm$ *SE* of three replicates. Each replicate represents at least 150 cells from 15 roots. (**C**) Schematic representation of normal and abnormal cross wall orientation. Cell walls that were perpendicular with the root axis (i.e. representing the angle $\geq 80°$ or $\leq 100°$) were scored as normally oriented, while angle $< 80°$ or $> 100°$ were scored as abnormal orientations. (**D**) Representative images of cross walls in WT BY-2 cells and overexpression of OsTTLL12-RFP BY-2 cells. (**E**) Statistical analysis of frequency distribution over the orientation of cross walls in WT BY-2 cells and overexpression of OsTTLL12-RFP BY-2 cells, data represent mean values $\pm$ *SE* of three replicates and each replicate represents 1,000 cells. (**F**) Representative images of phragmoplast microtubule orientation visualized by indirect immunofluorescence staining using monoclonal antibody DM1A in WT BY-2 cells and BY-2 cells overexpressing OsTTLL12-RFP, fluorescein iso-thiocyanate (FITC) as readout. OsTTLL12 is reported through the fused monomeric RFP.

the frequency of the abnormally oriented cell walls had increased significantly from around 20% in the WT to around 50% in all scored lines overexpressing of OsTTLL12. This phenotype could also be recapitulated in the overexpression of OsTTLL12-RFP BY-2 cells (Figure 7D), where the abnormal cell wall orientation was around 33% compared with 13% in WT BY-2 cells (Figure 7E). Thus, overexpression of OsTTLL12 led to disordered cell wall orientation.

During cytokinesis, the cell plate forms through the phragmoplast that consists of microtubule, actin, and other cellular components. The phragmoplast microtubules perpendicular to the cell axis and align two sides of the phragmoplast midzone, where the cell plate assembly occurs. The assembly of cell plate requires phragmoplast expansion, which depends on the dynamic instability of microtubules (Smertenko et al., 2017). We therefore asked whether overexpression of OsTTLL12 would

affect the organization of phragmoplast microtubules. We tested this implication in the OsTTLL12 overexpressor BY-2 cell line by immunofluorescence staining of phragmoplasts. As shown in Figure 7F, OsTTLL12 colocalized tightly with phragmoplast microtubules. In addition, the phragmoplast showed perturbations of alignment, where a wavy and even not contiguous phragmoplast midzone in OsTTLL12 overexpressor BY-2 cells when compared with WT BY-2 cells, also stained by immunofluorescence (Figure 7F, left) where the phragmoplast was aligned properly and perpendicular to the cell axis.

DISCUSSION

The only member of the TTL family present in plants seems to be TTLL12. To get insight into the function of tubulin

detyrosination and tyrosination cycle, we have, in the current study, overexpressed TTLL12 from rice in tobacco BY-2 cells as heterologous system (to follow the localization of OsTTLL12 during cell division), and in rice as homologous system (to probe for developmental functions of OsTTLL12). We observe (relatively subtle) changes in the orientation of cortical microtubules that correlate with modulations of growth. As the most specific phenotype, we can pinpoint a perturbed organization of the phragmoplast (in tobacco cells), and a perturbed organization of cross walls (in rice roots). We find that, unexpectedly, α-tubulin shifts towards the detyrosinated form upon overexpression of OsTTLL12. In the following, we discuss the significance of our finding with respect to the functional differentiation of different microtubule arrays, the role of post-translational modifications for the reorientation of cortical microtubules, and the organization of the phragmoplast. At the end we discuss, whether OsTTLL12 might be the elusive plant version of a tubulin tyrosine (de) carboxylase (TTC), or a plant unidentified plant TTL, and how we plan to follow up this idea in the future.

Why is it worth to study plant TTLs (or TTLL12s)?

Plant microtubules undergo a dynamic reorganization that is important for the axiality of cell division, cell growth, and differentiation (reviewed in Nick, 2007). This leads to the question, how tubulins target the different microtubule arrays that partially coexist in the same cell. The original idea that different arrays are composed of different tubulin isotypes has been discarded, based on the finding that microtubules utilize different isotypes simultaneously (Hussey et al., 1987). However, tubulin post-translational modification would provide an alternative mechanism to assign different functionalities to different microtubules occurring in the same cell. The highly conserved tyrosine at the carboxy-terminus of all eukaryotic tubulins (with exception of the slime mold *Physarum*, Watts et al., 1988) is evidence for the importance of tubulin detyrosination and tyrosination.

Plant TTLL12s are the only protein family with significant homology to animal TTLs. By their homology, they seem closer to animal TTLL12s. However, such conclusions come with a caveat, since the plant sequences possess an extension with a very long N-terminal LRR domain (Figures 1, S1) that is either absent (mammalian TTLs) or different (N-terminal SET-like domain in animal TTLL12). Nevertheless, as long as the enzymatic function of these plant proteins *in vitro* remains unknown, we will designate them as TTLL12. The LRR domain occurs in a large number of proteins and functions for specific protein–protein interactions, for instance in receptors (reviewed in Kobe and Kajava, 2001). This would indicate that the ligase function, located in the C-terminal half of the protein becomes active upon binding to specific interaction partners. These partners remain to be identified, for instance by pull-down assays using recombinantly expressed rice TTLL12, but already from the structural features a scenario emerges, where the tubulin ligase activity can be recruited to specific sites in the cell

through this LRR domain, a working hypothesis, we will pursue in future studies. In the current work, we have first probed for functional specificity of rice TTLL12.

Does OsTTLL12 bind to the detyrosinated form of α-tubulin?

OsTTLL12 was fused to a monomeric RFP (Campbell et al., 2002) such that can be used to study the localization of OsTTLL12 *in vivo*. By immunofluorescent labelling of microtubules in the OsTTLL12-RFP BY-2 cells, the RFP signal decorated all different microtubule arrays (Figure 2), suggesting that the RFP fusion obviously does not interfere with OsTTLL12 tubulin binding, which is consistent with maintained functionality. In contrast to the immunofluorescence labelling, *in vivo*, the RFP signals are mostly cytoplasmic, which may be the consequence of artificial overexpression of OsTTLL12-RFP driven by 35S promotor that covers the real localization. However, during immunofluorescence staining of microtubules, the excessive RFP signals are washed out such that masked cortical signals would emerge more clearly, which should make it easier to observe the RFP signals decorating the transverse and looser arrays of microtubules. A previous study (Wiesler et al., 2002) demonstrated that tyrosinated α-tubulin could be easily detected by monoclonal antibody ATT, but was not recognized by DM1A. However, upon cleavage of the C-terminal tyrosine by a C-terminal peptidase, the tubulin band became significantly smaller and ATT was no longer detecting this smaller tubulin, while this smaller tubulin became detectable by the monoclonal antibody DM1A. Indeed, DM1A recognizes an epitope located at amino acids 426–430, which is exposed in detyrosinated microtubules, but not in tyrosinated tubulin, while TTL is binding the C-terminal 10 amino acids (Kreis, 1987). The observations in the tobacco BY-2 overexpressor were congruent with those in the rice overexpressor. However, here we have observed a clear asymmetry in signal distribution when we assessed the localization of OsTTLL12 in the coleoptile epidermis, where cells are not cycling and where the cell wall already has developed a differentiated microfibril texture. Here, the oblique arrays in the rhizodermis harbor stable microtubules with a higher proportion of detyrosinated tubulin that is decorated by DM1A, while the loose arrays in the root cortex harbor more tyrosinated tubulin that are mainly decorated by OsTTLL12. This observed asymmetry indicates that there seems to be mutual competition between OsTTLL12 and antibody DM1A against detyrosinated α-tubulin, as would be expected if both bind to the C-terminus of α-tubulin.

A role for tubulin tyrosination status in microtubule orientation?

In epidermal cells of maize coleoptiles, stimulation of cell growth by auxin correlated not only with a reorientation of cortical microtubules to more transverse orientations, but also with a higher proportion of tyrosinated α-tubulin (Wiesler et al., 2002). Even within the same cell, during the reorientation, transverse

microtubules were preferentially composed of tyrosinated α-tubulin, while detyrosinated α-tubulin was more abundant in longitudinal microtubules. The differential modification of microtubules, depending on their orientation, may be caused by differences in turnover that would recruit TTC preferentially to the longitudinal microtubules (Kumar and Flavin, 1981), such that tubulins integrating into these longitudinal microtubules would get a higher chance to become detyrosinated ("stability first" model). However, there might as well be an inverse causality, where the detyrosinated α-tubulin would confer higher stability to the longitudinal arrays ("tubulin modification first" model). The analysis of the OsTTLL12 overexpressor lines allows to discriminate between the two possibilities: the overexpression resulted (unexpectedly) in a significant increase of detyrosinated over tyrosinated α-tubulin (Figures 5, 6), as well as in a reduced sensitivity to oryzalin (Figure 4). Because oryzalin eliminates microtubules by sequestering tubulin heterodimers from integration into growing microtubules (Morejohn et al., 1987), we can conclude that microtubules in the OsTTLL12 overexpressor are more stable than in the WT, which would correlate with a more pronounced detyrosination status, consistent with the results from Wiesler et al. (2002). Beyond the further confirmation of the correlation between detyrosinated α-tubulin and a more longitudinal orientation of microtubules, our observation bears on the differentiation between the "stability first" versus the "tubulin modification first" models. The genetically caused increase in tubulin detyrosination is probably the cause for the observed altered orientation of cortical microtubules in the overexpressor and not its consequence.

Interestingly, the effect of OsTTLL12 overexpression was different between coleoptile and root: in the coleoptiles, microtubules were shifted into a more transverse orientation (Figure 3F), which was correlated with increased mean cell length and longer coleoptiles (Figure 3A). The stimulation of cell elongation (note that after germination, coleoptiles grow exclusively by cell expansion) compensated for the decreased cell number (Figure 3B, E). In the root, the situation was inverse: here, microtubules were shifted into a steeper orientation (Figure 3C, F), followed by a reduction of growth. This is consistent with the data, where mitotic indices in rice roots decreased strongly and rapidly in response to nitro-tyrosine, causing an irreversible tyrosination of tubulin (Jovanovic et al., 2010). The most straightforward explanation of the shorter roots in the overexpressor of OsTTLL12 would assume, therefore, a shifted ratio of the two forms of tubulin as cause.

From these patterns, two conclusions can be drawn: (i) no matter in which direction microtubule orientation shifts as result of OsTTLL12 overexpression, the resulting organ growth remains linked with this orientation, namely the more transverse microtubules in the coleoptile support a stimulation of growth, the more longitudinal microtubules in the root inhibit growth; and (ii) the elevated detyrosination seen as a result of OsTTLL12 overexpression does not necessarily result in the same reorientation (steeper angles) of microtubules, but depends on the context. In the root, longitudinal

arrays are favored; in the coleoptile, transverse arrays are favored. Thus, detyrosination per se does not confer a particular orientation, it just seems to stabilize the respective orientation prevailing in the respective cells. This also means that detyrosination cannot be the only factor; it certainly integrates with other microtubular regulators, such as the increasing number of microtubule-associated proteins (comprehensively reviewed in Hamada, 2014). This finding represents a kind of extension of previous results (Wiesler et al., 2002), where detyrosination was associated with longitudinal microtubules that had been induced by auxin depletion. It would have been interesting to test whether a reversion of this experiment, where microtubules reorient from an originally longitudinal into a prospective transverse orientation by reincubation with auxin, would have led to the same outcome. Possibly, under these conditions it would have been the transverse microtubules that turn out to be detyrosinated preferentially.

Does tubulin retyrosination define functional subsets of microtubules? The case of the phragmoplast

Because plant cell shape is mainly under control of the cell wall, the abnormal cell wall orientations in the root meristem of OsTTLL12 overexpressor lines should lead to reduced root growth, which is congruent with our observations. Our data are also consistent with the previous report by Jovanovic et al. (2010), where nitro-tyrosine that conjugates to detyrosinated tubulin, but does so irreversibly affect cell wall organization in rice roots. The correct orientation of the new cell wall is predefined by the preprophase band as shown by elegant centrifugation experiments in fern protonemata (Murata and Wada, 1991), because the phragmoplast is organized by spatial cues from an endosomal belt organized by the preprophase band and persisting through mitosis (Dhonukshe et al., 2005). In the present work, we show that overexpression of OsTTLL12 in BY-2 cells leads to a perturbed phragmoplast (Figure 7F) contrasting with the strictly perpendicular and non-interrupted phragmoplast found in WT BY-2 cells (Figure 7F, WT). This indicates that overexpression of OsTTLL12 affects the structure of phragmoplast. This finding has matched with a report that during expansion, phragmoplast microtubules differing in dynamics act in concert. Hereby, dynamic microtubules mainly orient obliquely to the cell plate and nucleate via γ-tubulin more stable microtubules that are oriented mainly perpendicular to the cell plate; thus, the treadmilling of the dynamic microtubule population will drive the expansion of phragmoplast (Murata et al., 2013). Furthermore, phragmoplast microtubules interact with microtubule-associated proteins and kinesin motors. For instance, overexpression of OsKTN80a, a rice katanin P80 ortholog that acts as microtubule stabilizer, distorts phragmoplast microtubule organization (Wan et al., 2014). Mutations of class IV kinesins in the moss *P. patens* result in extended overlaps of microtubule plus-ends in the midzone of the phragmoplast followed by oblique orientation of cell plate (de Keijzer et al., 2017). Likewise, class XII

kinesins (Lee et al., 2007) and several class-XIV kinesins (Klotz and Nick, 2012; Buschmann et al., 2015) seem to participate in the organization of the phragmoplast. Because parthenolide, a drug that blocks the detyrosination function, promotes binding of the class XIV kinesin KCH to microtubules (Schneider et al., 2015), the observed perturbations of phragmoplast organization in the OsTTLL12 overexpressor may report a perturbed recruitment of specific kinesin motors to the phragmoplast. This would mean that tubulin tyrosination may define functional subpopulations of microtubules. To test this hypothesis, we are currently generating double-transformant lines, where OsTTLL12-RFP is present in the background of GFP-tagged microtubules, such that we can follow the interaction of OsTTLL12 with subsets of phragmoplast microtubules *in vivo*.

Is rice OsTTLL12 a rice TTL or TTC?

While purification and cloning of TTL from porcine brain was successful (Ersfeld et al., 1993), the TTC had remained enigmatic over 30 years. Only recently, the VASHs and their regulators the SVBPs were identified as the long-elusive TCPs (Aillaud et al., 2017; Nieuwenhuis et al., 2017). However, to the best of our knowledge, plant homologs of these animal TCPs are absent from plants, in contrast to TTL that deviate by their N-terminal extension, but otherwise are present in plants.

The direct product of a TTL should be tyrosinated α-tubulin, while the operational definition of a TTC is an enzymatic activity that yields detyrosinated α-tubulin. TTL prefers to bind to tubulin dimers (Kumar and Flavin, 1981) whereas TTC prefers assembled microtubules (Gundersen et al., 1987). These binding characteristics lead to the implication that the products of these two enzymes accumulate differently depending on the dynamics of microtubules. Stable microtubules should accumulate detyrosinated α-tubulin, whereas dynamic microtubules harbor more tyrosinated α-tubulin. However, in the present work, overexpression of OsTTLL12 yields more detyrosinated α-tubulin (Figures 5, 6) in the roots, and these roots show a higher stability against oryzalin, indicative of reduced turnover (Figure 4). Because higher detyrosination levels correlate with higher microtubule stability (resulting from the differential binding of TTL and TTC to dynamic vs. static microtubule populations), the outcome that overexpression of OsTTLL12 correlates with increased detyrosination is unexpected. The most straightforward interpretation would be that OsTTLL12 conveys the long-elusive TTC function. This interpretation would explain why overexpression of OsTTLL12 increased detyrosinated α-tubulin contents and conveyed higher stability of microtubule. In addition, the detyrosinated α-tubulin could act as initial signal that has effects on regulating tubulin synthesis (we currently pursue this in a detailed study that will be subject of a forthcoming paper). The observed higher tubulin contents due to overexpression of OsTTLL12 (Figure 6) may be involved in the mechanism of mutual regulation between post-translational modification and tubulin protein

OsTTLL12 affects microtubule dynamic and orientation synthesis (Breviario and Nick, 2000). In this context, the LRR domain (Figure S1) characteristic of plant TTLL12s may become interesting, because it implies that OsTTLL12 can form complexes with other proteins and because this LRR domain is different from animal SET-like domain. It is conceivable that such interactions may steer the direction of the enzymatic reaction (ligation of a tyrosine vs. cleavage of a tyrosine). To get biochemical access to the enzymatic activity conferred by TTLL12 and potential binding partners, we have launched recombinant expression for future *in vitro* studies.

MATERIALS AND METHODS

Multiple sequence alignment and phylogenetic analysis of TTLL12

The deduced TTLL12 from *Oryza sativa* ssp. *japonica* (Q8H022, Q10QY4 and Q10QY3), *Vitis vinifera* (A5AQ23), *Nicotiana tabacum* (A0A1S4CWA5), *Arabidopsis thaliana* (Q6IDC7, Q9CAQ1), the lycophyte *Selaginella moellendorffii* (D8RZ55), the bryophytes *Marchantia polymorpha* (A0A2R6WBW4), and *Physcomitrella patens* (A0A2K1KGF1), the chlorophyte *Chara braunii* (A0A388KR02), versus animals TTLL12, including *Danio rerio* (A0A0R4IKV1), *Homo sapiens* (Q14166), and *Mus musculus* (Q3UDE2), *Sus scrofa* (P38160) as well as the putative TTL from *Homo sapiens* (Q8NG68), and *Mus musculus* (P38585) from animals were collected from Swiss-Prot via a BLAST search. Sequences were aligned by KALIGN (https://msa.sbc.su.se/cgi-bin/msa.cgi), and the phylogenetic analysis was conducted by MEGA-6 (https://www.megasoftware.net/) using the Maximum Likelihood algorithm and a bootstrap consensus tree inferred from 100 replicates to represent the evolutionary history of the deduced proteins analyzed.

Cloning and transformation of rice and tobacco BY-2 cell

Total RNA was isolated from coleoptiles of *Oryza sativa* ssp. *japonica* cv. Dongjin using the innuPREP Plant RNA kit (Analytik Jena, Jena, Germany), and cDNA was synthesized by using the M-MuLV cDNA Synthesis Kit (New England Biolabs, Frankfurt, Germany) according to the instructions of the manufacturer by using 1 μg of total RNA as template. The full-length coding sequence of OsTTLL12 (SwissProt accession no. Q10QY4, LOC_Os03g08140.1, rice 2) was amplified by PCR using the oligonucleotide primers 5′-ATGTCGCCGGCCGCCGCCTC-3′ and 5′-TTACAGCGGCGATACATCTTTAAGC-3′ and integrated, after verification of the sequence, into the Gateway entry vector (Invitrogen, Paisley, UK). The insert was then transferred into the binary vector pH7WGR2 (N-terminal fusion of the red fluorescent protein, the constitutive CaMV 35S promoter, hygromycin resistance). The RFP was monomeric (Campbell et al., 2002). The resulting construct was then used for both stable transformations into rice plants and into tobacco BY-2 (*Nicotiana tabacum* L. cv Bright Yellow 2) cells.

Overexpression lines of OsTTLL12-RFP were generated in the rice (*Oryza sativa* L. ssp. *japonica*) cultivar "Dongjin" by

Agrobacterium-mediated transformation (Hiei et al., 1994); thus, the cultivar Dongjin was used as the WT control. Twenty independent lines were obtained, self-pollinated, and the next generation genotyped by genomic PCR for the presence of the RFP marker (using the primers 5′-CTTGGCCATGTAGG TGGTCT-3′ and 5′-CATCCCCGACTACTTGAAGC-3′) before picked for selfing. After at least five generations of self-pollination, the primary roots of three independent stable overexpression of OsTTLL12-RFP rice lines were harvested and used for expression analysis of the steady-state transcripts of OsTTLL12 by q-RT-PCR using pair primers (5′-GGGTTAGGT TAGCAAACAATCAGT-3′ and 5′-GTATCATATCCCGTATG CGTCCA-3′). The quantitative relative expression level of OsTTLL12 was calculated with the $2^{-\Delta\Delta C_t}$ method (Livak and Schmittgen, 2001) using rice glyceraldehyde 3-phosphate dehydrogenase (5′-AAGCCAGCATCCTATGATCAGATT-3′ and 5′-CGTAACCCAGAATACCCTTGAGTTT-3′) (Kumar et al., 2018) as internal reference gene for normalization.

Using the same vector, a tobacco BY-2 cell line stably overexpressing OsTTLL12-RFP (OsTTLL12) was also generated as described by Gao et al. (2016) using non-transformed BY-2 cells (WT) as control, selecting the transformants by 60 mg/L hygromycin.

Cultivation of plant and cell materials

Caryopses of WT and overexpression of OsTTLL12-RFP rice lines were preselected for uniformity and proper filling, and sown equidistantly on a floating plastic mesh in a box filled with 100 mL ddH$_2$O and cultivated at 25°C in photobiological darkness as described by Frey et al. (2010) for different time intervals depending on the respective experimental purposes.

Tobacco BY-2 cells were cultivated as described by Schneider et al. (2015). In addition to non-transformed tobacco BY-2 cells (WT), cells overexpressing OsTTLL12-RFP were used for co-localization and western blot analysis. The cultivation medium was complemented with 30 mg/L hygromycin.

Oryzalin treatment

Two sets of WT and three overexpression of OsTTLL12 rice seedlings were pre-selected with similar size and imaged at day 5 after sowing and root length at this time point (L_0) was measured by the periphery tool of Image J (NIH, Bethesda, USA; https://imagej.nih.gov). Then, one set was subjected to treatment with 100 nmol/Loryzalin (as treatment group), while the other set was cultivated without oryzalin (as control group) for an additional 24 h, before root tips were imaged by stereomicroscopy with a ×63 objective (Leitz, Diaplan, Bensheim, Germany) and root length and root tip width at this time point (L_1) determined. The relative growth rate (%) was determined as $\Delta L/L_0 \times 100\%$ with $\Delta L = L_1 - L_0$. The relative inhibition was calculated as |relative growth rate of treatment − relative growth rate of control|/growth rate of control. Three biological replicates were analyzed and each replicate was taken from nine individual roots.

Phenotyping of rice seedlings

If not stated otherwise, coleoptiles and roots were imaged at day 6 after sowing as described above. The length of coleoptile and primary root was measured by the periphery tool of Image J. Four biological replicates were analyzed with each replicate representing 15 individual seedlings. Mean cell length and cell number were determined as described by Frey et al. (2010) with minor modifications. Briefly, basal and apical parts of the coleoptile were separately immersed with one drop of 1 g/L Calcofluor White (Sigma, Darmstadt, Germany) and one drop 10% NaOH, and then the epidermal cells were imaged by fluorescence microscopy (AxioImager.Z1 Apotome, Zeiss, Jena, Germany, filter set 49 with excitation at 365 nm, beamsplitter at 395 nm, and emission at 445 nm at ×10 magnification). The mean cell length of epidermal cells in the basal and apical part of the coleoptile was determined by dividing the total length of one cell row to the numbers of cross walls counted along this row. The mean cell numbers were estimated by dividing the total length of coleoptile to the mean cell length. The data were collected from three independent replicates and each replicate was counted from a total of 350 cell profiles taken from 15 individual coleoptiles.

To determine the orientation of cross walls, seminal roots of WT and three independent overexpression of OsTTLL12-RFP lines were stained with 1% propidium iodide (Sigma, Steinheim, Germany) for 3 min, followed by washing twice with ddH$_2$O, before imaging the cells in the root apex by spinning disc microscopy. The angles between the cross wall and the lateral wall were measured by the angle tool of Image J. The data were collected from three independent replicates and for each replicate a total of 300 cells taken from 15 individual root were counted.

Antibodies used in this study

Microtubules (by immunofluorescence) and tubulin (by western blotting) were probed using two monoclonal mouse antibodies against α-tubulin. Antibody ATT was raised against tyrosinylated porcine brain α-tubulin that recognizes the C-terminal peptide VEGEGEEEGEEY (Kreis, 1987). Antibody DM1A was originally raised against chick-brain microtubules (Blose et al., 1984) and targets a conserved epitope DMAALEK (amino acid residues 424–430), which is exposed upon detyrosination of α-tubulin (Breitling and Little, 1986). Upon carboxyterminal cleavage native maize α-tubulin using carboxypeptidase A, this tubulin shifts in apparent size and becomes detectable by DM1A, but no longer by ATT (Wiesler et al., 2002): Thus, DM1A can be used to probe for detyrosinated α-tubulin.

Microtubule visualisation

Microtubules of rice coleoptiles and seminal root segments (either distal till 4 mm from the root tip, or proximal 3 mm–7 mm from the root tip) with or without oryzalin treatment were visualized by immunofluorescence (Abdrakhamanova et al., 2003) with minor modifications. Briefly, coleoptile and root segments were fixed by 3.7% w/v paraformaldehyde in microtubule stabilizing buffer (MSB: 0.05 mol/L PIPES, 0.005

mol/L EGTA, 0.001 mol/L MgSO4, 1% v/v glycerol, 0.25% v/v Triton-X 100, pH 6.9) for 1 h, while gently shaking. After fixation, 30 µm tangential sections were cut using a vibratome as described in (Abdrakhamanova et al., 2003). The sections were collected and placed on a glass slide in a drop of 1.2% w/v agar dissolved in MSB and then incubated with 5% v/v bovine serum albumin (Sigma, Neu-Ulm, Germany) in Tris-buffered saline (TBS: 0.15 mol/L NaCl, 0.02 mol/L Tris-HCl, 0.25% v/v Triton-X100, pH 7.4) for 20 min at 25°C to block non-specific interactions. After incubation overnight at 4°C with mouse monoclonal antibodies directed against α-tubulin (DM1A, Sigma, Neu-Ulm, Germany; dilution 1:100 in TBS), the sections were washed three times for 5 min with TBS. Then, they were reincubated for 1 h at 37°C with an FITC-conjugated secondary antibody (anti-mouse immunoglobulin G from goat; Sigma, Deisenhofen, Germany) diluted 1:20 in TBS. Sections were washed three times for 5 min in TBS and then imaged immediately. Depending on the angle between microtubules and side wall where 0° represented microtubule was perpendicular to side wall while 90° represented microtubule was parallel to side wall, the frequency of microtubule orientation was quantified from 435 cells in total from WT and from 450 cells from OsTTLL12 in four biological replicates.

The microtubules in OsTTLL12 BY-2 cells were visualized by immunofluorescence at the time of maximal mitotic activity, at day 3 after subcultivation as described by Schwarzerová et al. (2006).

Protein extraction and western blot analysis

Proteins were extracted from rice coleoptile as described in Wiesler et al. (2002) with the minor modification that each sample contained 5 µL of a Protease Inhibitor Cocktail (Sigma-Aldrich, München, Germany) while proteins from root segments (0.5 mm from root tip to differentiation zone) were extracted as described in Olinevich et al. (2002). In case of BY-2 cells, proteins were extracted at the time of maximal mitotic activity at day 3 after subcultivations according to Jovanovic et al. (2010).

Proteins were separated by SDS-PAGE, probed by western blotting, and the relative abundance of tyrosinated and detyrosinated α-tubulin quantified as described in Schneider et al. (2015). Briefly, the extracts were denatured at 95°C for 5 min, and equal amounts of total protein were loaded on three SDS-PAGE on 10% (w/v) polyacrylamide gels using prestained size markers (P7704S or P7712S; New England Biolabs, Frankfurt, Germany). One gel was stained with Coomassie Brilliant Blue to verify the equal loading of lanes, while the other two gels were subjected to western blotting. Tyrosinated α-tubulin and detyrosinated α-tubulin were detected by the monoclonal mouse antibodies ATT (T9028; Sigma-Aldrich, Darmstadt, Germany) and DM1A (T9026; Sigma-Aldrich, Darmstadt, Germany), respectively. To quantify the signal, after correction for background, the bands in the western blot were plotted using the plot profile function of Image J. The integrated density of each band was calculated relative to the value obtained from the control gel. The relative abundance was determined as the relative density of tyrosinated or detyrosinated α-tubulin in TTLL12 dividing the relative density of tyrosinated or detyrosinated α-tubulin in WT, respectively.

EPC sepharose chromatography

Soluble proteins were extracted from rice coleoptiles and roots as described in (Wiesler et al., 2002) with the minor modification that each sample contained 5 µL of a Protease Inhibitor Cocktail (Sigma-Aldrich, München, Germany). Tyrosinated and detyrosinated α-tubulin were fractionated based on their differential affinity with the antimicrotubular compound phenyl urethane (EPC) following the protocol described by Wiesler et al. (2002): an amino-ethyl group was linked to a CNBr-activated sepharose 4B matrix (Sigma-Aldrich, Darmstadt, Germany) by ethylene-diamine to yield amino-ethyl sepharose. The amino-ethyl sepharose was then coupled by carboxy-ethyl-N-phenylcarbamate that was synthesized from ethyl chloro-carbonate and 3-amino-benzoic acid to yield EPC sepharose. The fractionation was conducted in batch as described by Wiesler et al. (2002), by mixing first the extract with the matrix in a reaction tube, and separating matrix and eluent by short centrifugation (1 min, 15,000 g, 4°C) in a reaction tube (2 mL), using glass wool as filter to prevent the supernatant becoming contaminated by the matrix. Then, the bound protein was eluted by increasing ionic stringency. For each elution step, we mixed the eluent with the matrix, and then reseparated by centrifugation. Ionic stringency was progressively increased by adding KCl (0 mol/L, 0.05 mol/L, 0.1 mol/L, 0.15 mol/L, 0.2 mol/L, 0.25 mol/L, 0.3 mol/L, 0.35 mol/L, 0.4 mol/L, 0.45 mol/L, 0.5 mol/L, and 1 mol/L). After precipitation of the eluted fractions by tri-chloro-acetic acid, we adjusted the pH to neutral prior to processing for SDS-PAGE and western blotting. The data represent mean values from three biological replicates of coleoptiles and roots.

Spinning-disc confocal microscopy

Cell wall orientation (stained by propidium iodide), microtubules (stained by immunofluorescence) as well as OsTTLL12 (visualized by fusion with RFP) were analyzed by spinning-disc confocal microscopy (AxioObserver Z1 microscope (Zeiss, Jena, Germany), using a cooled digital CCD camera (AxioCam MRm), and a spinning-disc device (YOKOGAWA CSU-X1 5000) to collect z-stacks. The fluorescence from FITC was observed through the 488 nm emission line and the fluorescence from RFP and propidium iodide was observed through the 561 nm emission line of an Ar-Kr laser (Zeiss, Jena, Germany). Confocal images were recorded using a Plan-Apochromat 63x/1.44 DIC oil objective operated via the Zen 2012 (Blue edition) software platform.

CONFLICT OF INTERESTS

The authors declare that there are no conflict of interests.

AUTHOR CONTRIBUTIONS

K.Z., X.Z., and S.D. performed the primary experimental work. P.H., M-J.H., and G.A. generated the overexpressor OsTTLL12 rice lines. V.P.S. provided technical assistance in microscope operation. K.Z., M.R., and P.N. evaluated experimental design and performed data interpretation. K.Z. drafted the manuscript and P.N. edited the manuscript. All authors read and approved of its contents.

Edited by: Christopher J. Staiger, Purdue University, USA.

REFERENCES

Abdrakhamanova, A., Wang, Q.Y., Khokhlova, L., and Nick, P. (2003). Is microtubule disassembly a trigger for cold acclimation? Plant Cell Physiol. **44:** 676–686.

Aillaud, C., Bosc, C., Peris, L., Bosson, A., Heemeryck, P., Van Dijk, J., Le Friec, J., Boulan, B., Vossier, F., and Sanman, L.E. (2017). Vasohibins/SVBP are tubulin carboxypeptidases (TCPs) that regulate neuron differentiation. Science **358:** 1448–1453.

Barisic, M., e Sousa, R.S., Tripathy, S.K., Magiera, M.M., Zaytsev, A.V., Pereira, A.L., Janke, C., Grishchuk, E.L., and Maiato, H. (2015). Microtubule detyrosination guides chromosomes during mitosis. Science **348:** 799–803.

Blose, S.H., Meltzer, D.I., and Feramisco, J.R. (1984). 10-nm filaments are induced to collapse in living cells microinjected with monoclonal and polyclonal antibodies against tubulin. J. Cell Biol. **98:** 847–858.

Brants, J., Semenchenko, K., Wasylyk, C., Robert, A., Carles, A., Zambrano, A., Pradeau-Aubreton, K., Birck, C., Schalken, J.A., and Poch, O. (2012). Tubulin tyrosine ligase like 12, a TTLL family member with SET-and TTL-like domains and roles in histone and tubulin modifications and mitosis. PLoS One **7:** e51258.

Breitling, F., and Little, M. (1986). Carboxy-terminal regions on the surface of tubulin and microtubules epitope locations of YOL1/34, DM1A and DM1B. J. Mol. Biol. **189:** 367–370.

Breviario, D., and Nick, P. (2000). Plant tubulins: A melting pot for basic questions and promising applications. Transgenic Res. **9:** 383–393.

Buschmann, H., Dols, J., Kopischke, S., Peña, E.J., Andrade-Navarro, M.A., Heinlein, M., Szymanski, D.B., Zachgo, S., Doonan, J.H., and Lloyd, C.W. (2015). *Arabidopsis* KCBP interacts with AIR9 but stays in the cortical division zone throughout mitosis via its MyTH4-FERM domain. J. Cell Sci. **128:** 2033–2046.

Cai, G. (2010). Assembly and disassembly of plant microtubules: tubulin modifications and binding to MAPs. J. Exp. Bot. **61:** 623–626.

Campbell, R.E., Tour, O., Palmer, A.E., Steinbach, P.A., Baird, G.S., Zacharias, D.A., and Tsien, R.Y. (2002). A monomeric red fluorescent protein. Proc. Natl. Acad. Sci. USA **99:** 7877–7882.

de Keijzer, J., Kieft, H., Ketelaar, T., Goshima, G., and Janson, M.E. (2017). Shortening of microtubule overlap regions defines membrane delivery sites during plant cytokinesis. Curr. Biol. **27:** 514–520.

Dhonukshe, P., Mathur, J., Hülskamp, M., and Gadella, T.W. (2005). Microtubule plus-ends reveal essential links between intracellular polarization and localized modulation of endocytosis during division-plane establishment in plant cells. BMC Biol. **3:** 11.

Duckett, C.M., and Lloyd, C.W. (1994). Gibberellic acid-induced microtubule reorientation in dwarf peas is accompanied by rapid modification of an α-tubulin isotype. Plant J. **5:** 363–372.

Erck, C., Peris, L., Andrieux, A., Meissirel, C., Gruber, A.D., Vernet, M., Schweitzer, A., Saoudi, Y., Pointu, H., and Bosc, C. (2005). A vital role of tubulin-tyrosine-ligase for neuronal organization. Proc. Natl. Acad. Sci. USA **102:** 7853–7858.

Ersfeld, K., Wehland, J., Plessmann, U., Dodemont, H., Gerke, V., and Weber, K. (1993). Characterization of the tubulin-tyrosine ligase. J. Cell Biol. **120:** 725–732.

Frey, N., Klotz, J., and Nick, P. (2010). A kinesin with calponin-homology domain is involved in premitotic nuclear migration. J. Exp. Bot. **61:** 3423–3437.

Gao, N., Wadhwani, P., Mühlhäuser, P., Liu, Q., Riemann, M., Ulrich, A. S., and Nick, P. (2016). An antifungal protein from *Ginkgo biloba* binds actin and can trigger cell death. Protoplasma **253:** 1159–1174.

Gilmer, S., Clay, P., MacRae, T.H., and Fowke, L. (1999). Acetylated tubulin is found in all microtubule arrays of two species of pine. Protoplasma **207:** 174–185.

Gundersen, G.G., Khawaja, S., and Bulinski, J.C. (1987). Post-polymerization detyrosination of alpha-tubulin: a mechanism for sub-cellular differentiation of microtubules. J. Cell Biol. **105:** 251–264.

Hamada, T. (2014). Microtubule organization and microtubule-associated proteins in plant cells. Int. Rev. Cell Mol. Biol. **312:** 1–52.

Hiei, Y., Ohta, S., Komari, T., and Kumashiro, T. (1994). Efficient transformation of rice (*Oryza sativa* L.) mediated by Agrobacterium and sequence analysis of the boundaries of the T-DNA. Plant J. **6:** 271–282.

Hussey, P.J., TRAAS, J.A., GULL, K., and LLOYD, C.W. (1987). Isolation of cytoskeletons from synchronized plant cells: The interphase microtubule array utilizes multiple tubulin isotypes. J. Cell Sci. **88:** 225–230.

Janke, C., and Magiera, M.M. (2020). The tubulin code and its role in controlling microtubule properties and functions. Nat. Rev. Mol. Cell Biol. **21:** 307–326.

Janke, C., Rogowski, K., Wloga, D., Regnard, C., Kajava, A.V., Strub, J.-M., Temurak, N., van Dijk, J., Boucher, D., and van Dorsselaer, A. (2005). Tubulin polyglutamylase enzymes are members of the TTL domain protein family. Science **308:** 1758–1762.

Jovanovic, A.M., Durst, S., and Nick, P. (2010). Plant cell division is specifically affected by nitrotyrosine. J. Exp. Bot. **61:** 901–909.

Klotz, J., and Nick, P. (2012). A novel actin–microtubule cross-linking kinesin, NtKCH, functions in cell expansion and division. New Phytol. **193:** 576–589.

Kobe, B., and Kajava, A.V. (2001). The leucine-rich repeat as a protein recognition motif. Curr. Opin. Struct. Biol. **11:** 725–732.

Kreis, T.E. (1987). Microtubules containing detyrosinated tubulin are less dynamic. EMBO J. **6:** 2597–2606.

Kumar, D., Das, P.K., and Sarmah, B.K. (2018). Reference gene validation for normalization of RT-qPCR assay associated with germination and survival of rice under hypoxic condition. J. Appl. Genet. **59:** 419–430.

Kumar, N., and Flavin, M. (1981). Preferential action of a brain detyrosinolating carboxypeptidase on polymerized tubulin. J. Biol. Chem. **256:** 7678–7686.

Lee, Y.-R.J., Li, Y., and Liu, B. (2007). Two *Arabidopsis* phragmoplast-associated kinesins play a critical role in cytokinesis during male gametogenesis. Plant Cell **19**: 2595–2605.

Little, M., and Seehaus, T. (1988). Comparative analysis of tubulin sequences. Comparat. Bioche. Physiol. Part B: Comparat. Biochem. **90**: 655–670.

Livak, K.J., and Schmittgen, T.D. (2001). Analysis of relative gene expression data using real-time quantitative PCR and the 2− ΔΔCT method. Methods **25**: 402–408.

Morejohn, L.C., Bureau, T.E., Molè-Bajer, J., Bajer, A.S., and Fosket, D.E. (1987). Oryzalin, a dinitroaniline herbicide, binds to plant tubulin and inhibits microtubule polymerization. *in vitro*. Planta **172**: 252–264.

Murata, T., Sano, T., Sasabe, M., Nonaka, S., Higashiyama, T., Hasezawa, S., Machida, Y., and Hasebe, M. (2013). Mechanism of microtubule array expansion in the cytokinetic phragmoplast. Nat. Commun. **4**: 1967.

Murata, T., and Wada, M. (1991). Effects of centrifugation on pre-prophase-band formation in *Adiantum protonemata*. Planta **183**: 391–398.

Nick, P. (2007). Control of cell axis. *Plant Microtubules (Springer)*. pp. 3–46.

Nieuwenhuis, J., Adamopoulos, A., Bleijerveld, O.B., Mazouzi, A., Stickel, E., Celie, P., Altelaar, M., Knipscheer, P., Perrakis, A., and Blomen, V.A. (2017). Vasohibins encode tubulin detyrosinating activity. Science **358**: 1453–1456.

Olinevich, O.V., Khokhlova, L.P., and Raudaskoski, M. (2002). The microtubule stability increases in abscisic acid-treated and cold-acclimated differentiating vascular root tissues of wheat. J. Plant Physiol. **159**: 465–472.

Peris, L., Wagenbach, M., Lafanechère, L., Brocard, J., Moore, A.T., Kozielski, F., Job, D., Wordeman, L., and Andrieux, A. (2009). Motor-dependent microtubule disassembly driven by tubulin tyrosination. J. Cell Bio. **185**: 1159–1166.

Prota, A.E., Magiera, M.M., Kuijpers, M., Bargsten, K., Frey, D., Wieser, M., Jaussi, R., Hoogenraad, C.C., Kammerer, R.A., Janke, C., and Steinmetz, M.O. (2013). Structural basis of tubulin tyrosination by tubulin tyrosine ligase. J. Cell Biol. **200**: 259–270.

Schneider, N., Ludwig, H., and Nick, P. (2015). Suppression of tubulin detyrosination by parthenolide recruits the plant-specific kinesin KCH to cortical microtubules. J. Exp. Bot. **66**: 2001–2011.

Schwarzerová, K., Petrášek, J., Panigrahi, K., Zelenková, S., Opatrný, Z., and Nick, P. (2006). Intranuclear accumulation of plant tubulin in response to low temperature. Protoplasma **227**: 185–196.

Smertenko, A., Assaad, F., Baluška, F., Bezanilla, M., Buschmann, H., Drakakaki, G., Hauser, M.-T., Janson, M., Mineyuki, Y., and Moore, I. (2017). Plant cytokinesis: Terminology for structures and processes. Trends Cell Biol. **27**: 885–894.

Smertenko, A., Blume, Y., Viklický, V., Opatrný, Z., and Dráber, P. (1997). Post-translational modifications and multiple tubulin isoforms in *Nicotiana tabacum* L. cells. Planta **201**: 349–358.

Wan, L., Wang, X., Li, S., Hu, J., Huang, W., and Zhu, Y. (2014). Overexpression of OsKTN80a, a katanin P80 ortholog, caused the repressed cell elongation and stalled cell division mediated by microtubule apparatus defects in primary root in *Oryza sativa*. J. Integr. Plant Biol. **56**: 622–634.

Wang, W., Vignani, R., Scali, M., Sensi, E., and Cresti, M. (2004). Post-translational modifications of alpha-tubulin in *Zea mays* L are highly tissue specific. Planta **218**: 460–465.

Wasylyk, C., Zambrano, A., Zhao, C., Brants, J., Abecassis, J., Schalken, J.A., Rogatsch, H., Schaefer, G., Pycha, A., and Klocker, H. (2010). Tubulin tyrosine ligase like 12 links to prostate cancer through tubulin posttranslational modification and chromosome ploidy. Int. J. Cancer **127**: 2542–2553.

Watts, D.I., Monteiro, M.J., and Cox, R.A. (1988). Identification of EcoRV fragments spanning the Nα-tubulin gene of *Physarum*. FEBS Lett. **241**: 229–233.

Wiesler, B., Wang, Q.Y., and Nick, P. (2002). The stability of cortical microtubules depends on their orientation. Plant J. **32**: 1023–1032.

SUPPORTING INFORMATION

Additional Supporting Information may be found online in the supporting information tab for this article: http://onlinelibrary.wiley.com/doi/10.1111/jipb.13059/suppinfo

Figure S1. Multiple alignment of tubulin tyrosine ligase (TTL) homologs from different animals and plants

Figure S2. Phenotype of coleoptile and root growth after 6 d germination

(**A**) Representative images of 6 d old seedlings of wild type (WT) and three overexpression of OsTTLL12-RFP rice lines. Statistic analysis of (**B**) coleoptile and (**C**) primary root length of WT and three overexpression of OsTTLL12-RFP rice lines as showed in (**A**). Data represent mean values $\pm$ *SE* of three replicates, $n \geq 12$.

Figure S3. Root tips with or without 100 nM oryzalin treatment

(**A**) Representative images of root tips with or without 100 nM oryzalin treatment in wild type (WT) and three overexpression of OsTTLL12-RFP rice lines. (**B**) Statistic analysis of width of root tips with or without 100 nM oryzalin treatment as showed in (**A**). Data represent mean values $\pm$ *SE* of three replicates, $n = 13$.

Figure S4. Cellular localization of OsTTLL12-RFP in live cells

(**A**) Localization of OsTTLL12-RFP in cytoplasm of BY-2 cells overexpressing OsTTLL12-RFP. Bar, 10 μm. (**B**) Live-cell images of OsTTLL12-RFP in cells of apical meristem zone of overexpression of OsTTLL12-RFP rice line. Bar, 10 μm.

Figure S5. Phenotype of overexpression of OsTTLL12-RFP rice line

(**A**) 14 d old plants of wild type (WT) and overexpression of OsTTLL12-RFP rice line. Bar, 2 cm. (**B**) Statistic analysis of plant height and root length as showed in (**A**). Data represent mean values $\pm$ *SE* of three replicates, $n \geq 12$. (**C**) 60 d old plants of WT and overexpression of OsTTLL12-RFP rice line. α represent the tiller angle between the red line as showed in (**C**). Bar, 10 cm. (**D**) Statistic analysis tiller angle as showed in (**C**). Data represent mean values $\pm$ *SD* of 15 individual plants.

Figure S6. Tyrosinated and detyrosinated α-tubulin detected by western blot in WT and overexpressor OsTTLL12 BY-2 cells

CBB, Coomassie brilliant blue stained sodium dodecyl sulfate gel as control; Detyr-Tub, detyrosinated α-tubulin detected by DM1A; tyr-Tub, tyrosinated α-tubulin detected by ATT.

Scan using WeChat with your
smartphone to view JIPB online

Scan with iPhone or iPad to
view JIPB online